Doppler Polarimetric Radar Measurements of the Gamma Drop Size Distribution of Rain

H. W. J. RUSSCHENBERG

Department of Electrical Engineering, Delft University of Technology, Delft, the Netherlands

(Manuscript received 16 October 1992, in final form 29 May 1993)

ABSTRACT

The conversion of radar reflections into rain intensities is dependent upon assumptions regarding the drop size distribution. The gamma drop size distribution contains three unknown parameters; the number of parameters that can be obtained depends on the number of radar observables. When only the reflectivity is measured, one parameter is derived, combining it with the differential reflectivity results in the retrieval of two parameters, and when Doppler measurements are done as well, a third parameter is obtained. The Doppler spectrum may be distorted by turbulence; a correction procedure is developed. The combination of copolar and cross-polar radar measurements is used to estimate the canting-angle distribution. Analysis of data of the Delft atmospheric research radar during a moderate event shows that the three parameters of the gamma drop size distribution are statistically related. Combining these relationships results in an event-specific Z–R relationship.

1. The microstructure of rain

The microstructure of rain is determined by the statistical distributions of the size, shape, orientation, and fall speed of the drops. Of these, the fall speed v and particle shape D are uniquely related to the drop size, leaving only the drop size and orientation as independent parameters (Atlas et al. 1973). The drop size distribution $N(D)$ is given by the gamma distribution, while the orientation follows a Gaussian distribution $t(\delta)$ (Ulbrich 1983):

$$N(D) = N_0 D^{\mu} \exp\left(-\frac{3.67 + \mu}{D_0} D\right) \quad (1)$$

$$t(\delta) = \frac{1}{\sigma_\delta (2\pi)^{1/2}} \exp\left[-\frac{(\delta - \bar{\delta})^2}{2\sigma_\delta^2}\right]. \quad (2)$$

The variable D_0 is the diameter of the median drop volume, N_0 is a scaling factor, and μ is the dispersion factor; σ_δ is the width of the canting-angle distribution. The orientation angle δ is defined with respect to the vertical. The particles are assumed to be canted in a plane perpendicular to the plane containing the propagation vector of the radar wave. The mean orientation angle $\bar{\delta}$ is usually small (Brussaard 1976) and in this study set to 0°. The relationship between fall speed and drop size is given by (Atlas et al. 1973)

$$v(D) = 9.6 - 10.3 \exp(-0.6D) \quad (\mathrm{m\ s^{-1}}), \quad (3)$$

where D is in millimeters.

The volume Vol_t of the total water amount is given by

$$\mathrm{Vol}_t = \frac{\pi}{6} \int_0^{D_{\max}} D^3 N(D) dD \quad (4)$$

and the rain intensity R by

$$R = \frac{\pi}{6} \int_0^{D_{\max}} D^3 N(D) v(D) dD. \quad (5)$$

2. The radar observables

The Doppler spectrum $S_v(v)$ can be described by its statistical moments. Of these, the mean radial velocity V_d and the width $W_{d,m}$ are used in this paper:

$$V_d = \frac{1}{Z_d} \int_{V_{\min}}^{V_{\max}} v S_v(v) dv \quad (6)$$

$$W_{d,m} = \left[\frac{1}{Z_d} \int_{V_{\min}}^{V_{\max}} (v - V_d)^2 S_v(v) dv\right]^{1/2} \quad (7)$$

with

$$Z_d = \int_{V_{\min}}^{V_{\max}} S_v(v) dv \quad (8)$$

as the mean backscattered power. Apart from the fall speed of raindrops, the width of the Doppler spectrum may also contain contributions from turbulence, wind shear, drop vibration, or wind gusts (Doviak and Zrnić 1984). In this paper, W_d is used to describe the contribution of fall speed of raindrops. The measured spectrum width $W_{d,m}$ is then given by

Corresponding author address: Dr. H. W. J. Russchenberg, Department of Electrical Engineering, Delft University of Technology, Microwave Laboratory, P.O. Box 5031, 2600 GA Delft, the Netherlands.

$$W_{d,m} = (W_d^2 + W_t^2)^{1/2}, \quad (9)$$

with the effect of the other contributions to the Doppler spectrum lumped into W_t. In this paper, W_t is referred to as the width of the turbulence spectrum. The polarimetric radar measurements of precipitation can be expressed by several radar observables. The most familiar is the *horizontal reflectivity* Z_h, which is copolarly measured with horizontal polarization. The polarization dependence of the radar signal is described by the *differential reflectivity* Z_{DR} and the *linear depolarization ratio* L_{DR}:

$$Z_h = \int \sigma_{hh}(D, \delta)N(D)t(\delta)dDd\delta \quad (10)$$

$$Z_{DR} = \frac{Z_h}{Z_v} = \frac{\int \sigma_{hh}(D, \delta)N(D)t(\delta)dDd\delta}{\int \sigma_{vv}(D, \delta)N(D)t(\delta)dDd\delta} \quad (11)$$

$$L_{DR} = \frac{Z_{hv}}{Z_v} = \frac{\int \sigma_{hv}(D, \delta)N(D)t(\delta)dDd\delta}{\int \sigma_{vv}(D, \delta)N(D)t(\delta)dDd\delta}, \quad (12)$$

with σ_{kl} as the radar cross section measured with transmitted polarization k and received polarization l. In this paper the frequency of the Delft atmospheric research radar, 3.315 GHz, is used to calculate the radar observables. Polarimetric observations of rainfall are optimally performed with the radar pointed toward the horizon. Doppler measurements, however, must be done with the radar pointed toward the zenith. To combine the two, the radar elevation must be set to a position in-between. In this paper, 30° with respect to the horizontal is used.

3. Existing methods for radar-based prediction of the rain intensity

When one-parameter radar systems are used to obtain the rain intensity R, a power law that relates the measured reflectivity Z to it is applied,

$$Z = \alpha R^\beta, \quad (13)$$

in which α and β are constants that depend on the drop size distribution. The polarization dependence, and hence the effect of particle shape, is ignored. Usually α and β are derived from long-term statistics of rainfall, while their instantaneous values may differ from event to event, and from place to place. Both Z and R are sensitive to the drop size distribution, and so the Z–R relationship depends on the type of rain. Battan (1973) lists 69 Z–R relationships that are derived at various locations throughout the world. As was shown by Ulbrich (1983), relationships of the form of (13) are based on the assumptions of a constant N_0 and μ; D_0 is the running parameter. With the advent of multiparameter radar, however, the accuracy of the radar-derived rain intensity may be increased, because more parameters of the drop size distribution can be obtained. Klaassen (1989) used a vertically pointed Doppler radar to obtain N_0 and D_0 of the drop size distribution with $\mu = 0$, and calculated the rain intensity. To this end, three Doppler spectrum parameters were defined that correspond to the minimum, mean, and maximum velocity of the raindrops. The method relies heavily on the presence of large drops and can therefore be used only during events with a high rain intensity. While Klaassen parameterized the Doppler spectrum by three velocities, Hauser and Amayenc (1981) used curve-fitting techniques during similar experiments to obtain N_0 and D_0 from a best fit of the theoretical to the measured Doppler spectrum. Both methods are very sensitive to the vertical wind speed. Therefore, they lose their applicability in convective storms, where strong up- and downdrafts disturb the Doppler spectrum too much. To overcome the dependence on the mean wind speed, the width of the Doppler spectrum will be used in this paper to characterize the drop size distribution. The vertical air velocity can be measured directly by wind profilers. These are UHF and VHF radars that measure wind fields, but an increasing effort is put into using them to estimate the rain intensity as well (Chu et al. 1990). Steiner (1991) used Z_{DR} to estimate the fall speed of raindrops, which, when combined with Doppler radar measurements, may improve radar measurements of the rain intensity. Fujita et al. (1989) report on the use of a dual-wavelength radar to estimate the rain intensity, employing a long wavelength that does not suffer from attenuation by rain, and one that does. The ratio of the two return powers depends only on the attenuation and is converted into the rain intensity, using well-known power laws. The method is favorable for deriving R from a fixed Z–R relationship, but in case of strong rain cells the short-wavelength radar signal may be attenuated too much to allow a correct conversion. Also, long time and range integration is necessary to obtain sufficient accuracy. Seliga and Bringi (1976) gave a strong impulse to the use of multiparameter radar systems by suggesting the use of orthogonal polarizations for measuring precipitation: combining the differential reflectivity with the horizontal reflectivity significantly increases the accuracy of rainfall measurements. Steinhorn and Zrnić (1988) suggest the use of the differential propagation phase shift K_{DP} to improve the estimate of the drop size distribution; K_{DP} is defined as the difference of the propagation phase shifts at horizontal and vertical polarization of the radar wave. Since K_{DP} depends on the particle shape, it will also depend on the drop size distribution. By combining K_{DP} with Z_h and Z_{DR}, these parameters of the drop size distribution can be obtained, but the method poses strong demands on the accuracy of the measured differential phase shift (which

may be achieved only after long time and range integration). The Z–R relationship may be replaced by a Z_h–K_{DP} relationship to improve rainfall estimations and to discriminate rain and hail.

This paper will deal with an alternative method to characterize the three parameters of the drop size distribution. The combination of Z_{DR} and W_d will be used to obtain μ. The corresponding D_0 is derived from Z_{DR}, and in the last step Z_h is used to obtain N_0. The last two steps follow the approach of Seliga and Bringi (1976), which will be discussed in the next section.

4. Deriving N_0 and D_0 from Z_h and Z_{DR}

The variable Z_{DR} is independent of N_0; when $t_\delta(\delta)$ and μ are known, measurement of Z_{DR} directly results in D_0. The obtained D_0 is incorporated into (10) to derive N_0 from the measured Z_h. Finally, N_0 and D_0 are used to calculate the rain intensity. The relationship between drop size and shape is important, for it is the base of conversion of Z_{DR} into D_0. In this study the results of Pruppacher and Pitter (1971), based on wind tunnel experiments, are used.

The Z_h–Z_{DR} method to estimate the drop size distribution assumes a constant dispersion factor and known particle orientation. However, both may change during the event, thereby affecting the accuracy of the radar-derived rain intensity. To simplify calculations of the effect of μ variations on the derived rain intensity, the particles are considered to be spheres. When $D_{max} \to \infty$, the ratio of Z and R is given by (Russchenberg 1992)

$$\frac{Z}{R} = \frac{(\mu + 6)![D_0/(3.67 + \mu)]^{\mu+3}}{(\mu + 3)!\{9.65 - 10.3 \times [(3.67 + \mu)/(3.67 + \mu + \alpha D_0)]^{\mu+4}\}}, \quad (14)$$

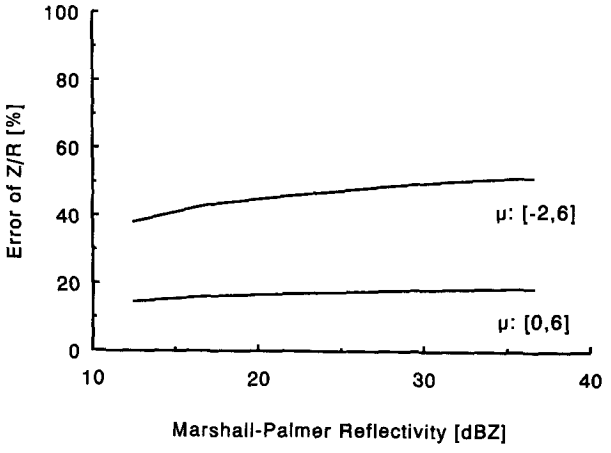

FIG. 1. The relative error of Z/R due to variation of the dispersion factor μ versus $Z = 200\ R^{1.6}$; μ varies between [0, 6], or [−2, 6].

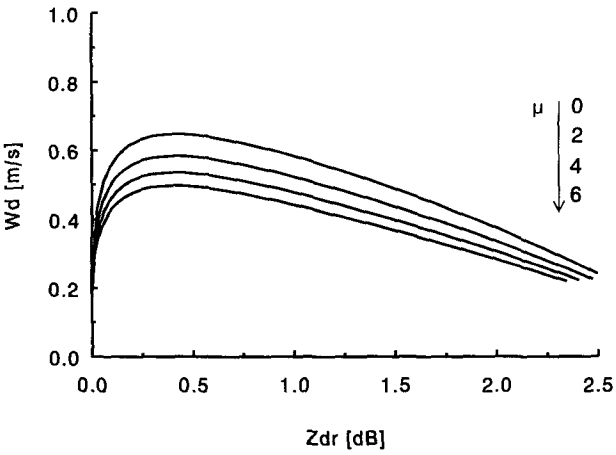

FIG. 2. The spread of the Doppler spectrum W_d versus the differential reflectivity Z_{DR} for different values of the dispersion factor μ. The radar elevation angle is set to 30°.

with $\alpha = 0.6$. After D_0 is obtained from Z_{DR} for some fixed value of μ, (14) can be used to derive R from the measured Z. To estimate the standard deviation of Z/R one must know the range of values μ that may occur. Ulbrich (1983), Bringi et al. (1983), and Goddard and Cherry (1984) mainly reported values of μ between 0 and 5, although negative values may occur as well. Figure 1 shows the relative error, defined as the standard deviation normalized to the mean, of Z/R as function of the reflectivity that corresponds to the Z–R relationship of the Marshall–Palmer distribution, $Z = 200R^{1.6}$. The range of variation of μ is either set to [−2, 6] or [0, 6]. In the former case the error varies between 35% and 55%, while in the latter it is confined to 15%–20%.

5. Deriving μ from Z_{DR} and W_d

In Fig. 2, W_d is plotted versus Z_{DR} for μ varying between 0 and 6. If there is sufficient accuracy, a combined measurement of Z_{DR} and W_d can be converted into a value of μ. An analytical expression of W_d as function of Z_{DR} and μ is difficult to derive, which necessitates numerical techniques to investigate the accuracy of the method to determine μ. The accuracy depends on several factors, related to the rain model used and to the statistical nature of rain. To begin with the model-related factors, the accuracy may be affected by the choice of the maximum diameter D_{max} and the spread of the canting-angle distribution; D_{max} affects W_d as well as Z_{DR}; turbulence directly affects the Doppler spectrum and may also influence Z_{DR} because of the particle canting it may cause. The influence of D_{max} is insignificant as long as $D_{max}/D_0 > 2.5$ (Ulbrich 1983). This requirement is often satisfied, because $D_0 < 2$ mm and $D_{max} \simeq 8$ mm (Pruppacher and Pitter 1971). It is also likely that D_{max} increases with increas-

ing D_0, thereby decreasing the probability of $D_{max}/D_0 < 2.5$.

The derivation of D_0 from Z_{DR} relies on a priori knowledge of σ_δ, the spread of the canting-angle distribution. To estimate σ_δ, a combined measurement of Z_{DR} and L_{DR} can be used. However, in that case a priori knowledge of the dispersion factor is needed. Joss and Gori (1978) showed that *long-term* integrated drop size distributions can be represented with $\mu = 0$.

Turbulence can increase the width of the Doppler spectrum, and, if so, must be corrected for. However, instantaneous correction of the Doppler spectrum for turbulence is not feasible. In this paper, the correction is achieved after long-term integration of the radar observables. Assuming $\mu = 0$, the long-term averaged Z_{DR} is used to estimate the median drop size, which is used to calculate W_d; W_d is compared with the spread $W_{d,m}$ of the measured spectrum, and finally, the spread W_t of the turbulence spectrum results. The thus obtained long-term averaged W_t is used for *samplewise* correction of the measured signal. In the sections concerning the data analysis, the error of the derived drop size distribution due to this scheme is discussed.

The long-term integration is necessary for two reasons: 1) to estimate σ_δ from Z_{DR} and L_{DR} a priori knowledge of μ is needed, and 2) correction of the Doppler spectrum for turbulence cannot be done instantaneously. Using a radar-derived value of σ_δ as done in this paper differs from the conventional method of using Z_{DR} alone to estimate rainfall, for then σ_δ is assumed to be fixed for all events.

Assuming $D_{max} \to \infty$, the change of W_d due to a change $\Delta\mu$ of μ is given by (Russchenberg 1992)

$$\Delta W_d = \frac{1}{2W_d}(\mathcal{F}_1 - \mathcal{F}_2)\Delta\mu \tag{15}$$

with $\mathcal{F}_1$ and $\mathcal{F}_2$ equal to

$$\mathcal{F}_1 = \exp[(\mu+7)\mathcal{G}_1] \times \left\{\mathcal{G}_1 + \left[\frac{1.2D_0(\mu+7)}{(3.67+\mu+1.2D_0)(3.67+\mu)}\right]\right\} \tag{16}$$

$$\mathcal{F}_2 = \exp[(\mu+7)\mathcal{G}_2] \times \left\{\mathcal{G}_2 + \left[\frac{1.2D_0(\mu+7)}{(3.67+\mu+0.6D_0)(3.67+\mu)}\right]\right\} \tag{17}$$

and

$$\mathcal{G}_1 = \ln\left(\frac{3.67+\mu}{3.67+\mu+1.2D_0}\right) \tag{18}$$

$$\mathcal{G}_2 = 2\ln\left(\frac{3.67+\mu}{3.67+\mu+0.6D_0}\right). \tag{19}$$

The relative change $\Delta x_{rel}(\mu)$ of a variable x is related to $\Delta x(\mu)$ by

$$\Delta x_{rel}(\mu) = 10\log\left[1 + \frac{\Delta x(\mu)}{x(\mu)}\right]. \tag{20}$$

Figure 3 shows the μ dependence of the relative change of W_d and Z_{DR}, referred to as $\Delta Z_{DR,rel}$ and $\Delta W_{d,rel}$ due to $\Delta\mu = +1$: $D_0 = 1$, 1.5, or 2 mm. The change of Z_{DR} with respect to changes of μ was derived numerically, with Z_{DR} expressed in decibels; W_d is expressed in meters per second. The elevation angle of the radar is set to 30°.

The term $\Delta Z_{DR,rel}$ varies between −1.8 and −0.1 dB; it decreases for larger values of μ; $\Delta Z_{DR,rel}$ is negative due to the fact that Z_{DR} decreases with increasing μ; $\Delta W_{d,rel}$ is smaller: $-0.1 < \Delta W_{d,rel}(\mu) < 0.4$ dB. It is negative for small μ, and positive for large μ. When D_0 increases, the relative changes decrease.

The stochastic nature of rain influences the measurement accuracy of Z_{DR} and $W_{d,m}$. The accuracy of Z_{DR} measurements is described by Bringi et al. (1983). Doviak and Zrnić (1984) discuss the measurement accuracy of $W_{d,m}$. The signal processing of the Delft atmospheric research radar is discussed by Russchenberg (1992). The initial measurement accuracy of Z_{DR} equals 1.1 dB, and that of $W_{d,m}$ varies between 0.1 and 0.2 dB. The error in $W_{d,m}$ decreases with increasing $W_{d,m}$. After additional integration of 200 samples, the relative errors are much smaller: that of Z_{DR} is less than 0.1 dB, and that of $W_{d,m}$ even smaller. For the data used in this paper, the integration is achieved by integrating over 20 time samples and 10 range cells; the integration time equals 64 s, and the integration range is 1500 m.

6. Measurements

The Delft atmospheric research radar is located in an urbanized area near the coast of the Netherlands.

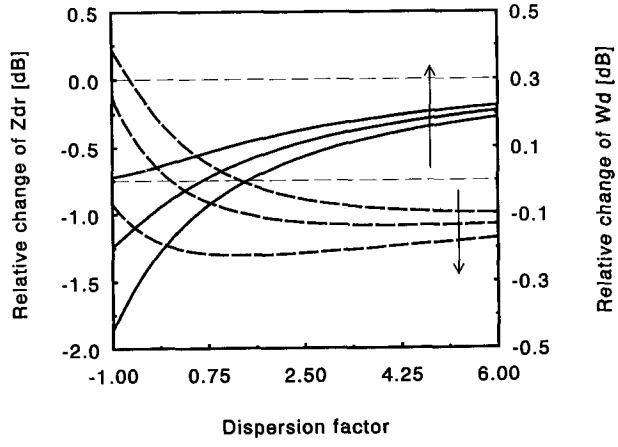

FIG. 3. The relative change of the differential reflectivity Z_{DR} (solid line) and the spread of the Doppler spectrum W_d (dashed line) due to $\Delta\mu = 1$ as function of the dispersion factor μ. In the direction of the arrow, D_0 is set to 1, 1.5, and 2 mm. Note the different scales.

The meteorological and experimental conditions during the measurements are given in Table 1. Figure 4 shows the time dependence of the radar observables during approximately 1.5 h. The data are integrated over 64 s and 300 m in range. Initially, the antennas were pointed approximately perpendicular to the mean wind direction; halfway through the measurement the antennas were rotated 10° in the horizontal plane, implying a horizontal shift of the range cell under consideration of about 130 m. In the data, the antenna rotation reveals itself through a change of L_{DR}, $W_{d,m}$, and V_d; V_d is very small before the rotation, as expected, because only the radial component of the wind speed is measured, but after the rotation V_d is increased to approximately 5 m s^{-1} (toward the radar), indicating strong wind between 15 and 20 m s^{-1}; $W_{d,m}$ is increased as well; on average from 1.1 to 1.4 m s^{-1}. Since no significant change of Z_h and Z_{DR} is observed, it is unlikely that rain has caused the change of $W_{d,m}$; $W_{d,m}$ is larger than could be caused by the fall speed of raindrops alone (see also Fig. 2), and considering the azimuth dependence, turbulence may have been of influence. Anisotropic atmospheric turbulence has often been observed under clear-air conditions by wind profilers and is considered to be caused by atmospheric layers in which turbulent wind flows propagate (Woodman and Chu 1989). Most wind profiler data represent high altitudes, but the measurements described in this paper show similar phenomena in the lower troposphere.

The observed values of L_{DR}, although well above the antenna limit of the radar (see Table 1), are significantly larger than measured with the Chilbolton radar (Frost et al. 1991); L_{DR} is correlated to $W_{d,m}$ during the antenna rotation, L_{DR} increases approximately 2 dB, indicating some relationship with turbulence.

The horizontal reflectivity Z_h fluctuates around 30 dBZ, corresponding to approximately 3 mm h^{-1}; Z_{DR} fluctuates around 0.4 dB. After approximately 55 min a large peak value of Z_{DR} occurs, accompanied by a peak of Z_h. As was explained before, the necessary accuracy requires substantial integration of the radar signals. Although not shown, increasing the integration range to 1500 m only made the figure slightly smoother; the spatial structure of the rain region appears to be reasonably homogeneous.

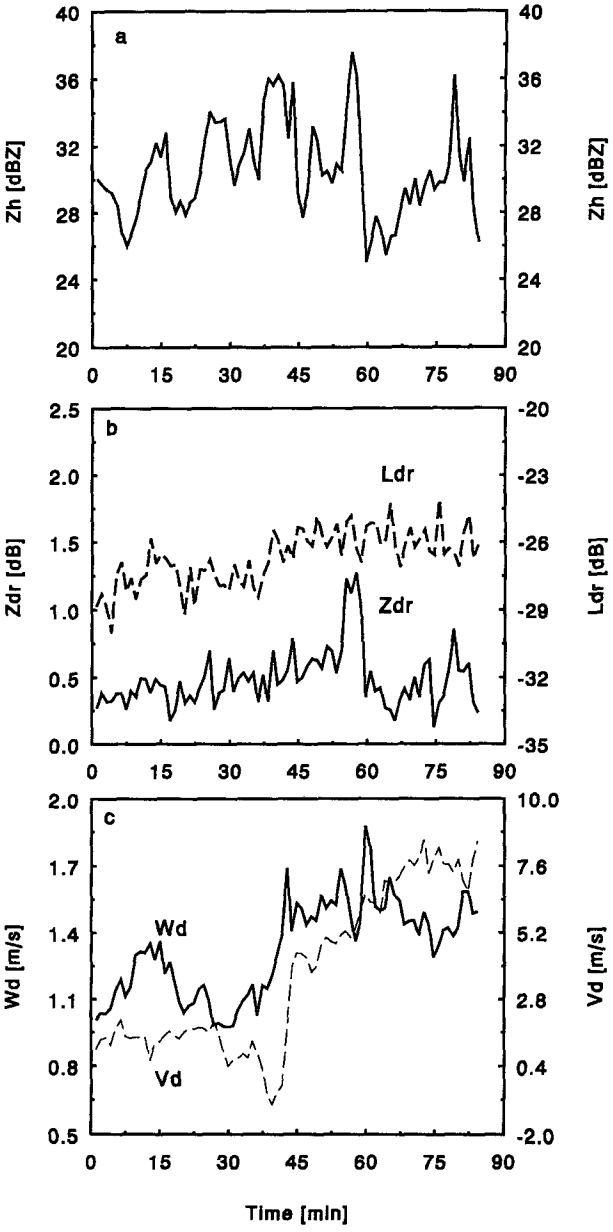

FIG. 4. Time dependence of the radar observables, averaged over 64 s and 300 m. Altitude: 850 m.

TABLE 1. The meteorological and experimental conditions during the radar measurements.

Ground temperature	10°C
0°C isotherm	1800 m
Mean wind speed	15–20 m s^{-1}
Mean wind direction	Southwest
Weather type	Cold front
Rain intensity	±3 mm h^{-1}
Maximum radar range	9600 m
Range resolution	150 m
Radar elevation	30°
Maximum Doppler velocity	±9 m s^{-1}
Signal-to-noise ratio	>20 dB
Minimum detectable L_{DR}	−31 dB

The first step in the procedure to derive the dispersion factor is the correction of the Doppler spectrum for turbulence: the data must be integrated over a sufficiently long period. Due to the rotation of the antennas the first and second half of the measurement must be treated separately. The integration of the second part of the measurement is done with exclusion of the peak value of Z_{DR} to avoid biasing by one dominant

measurement. The first part is integrated over 42 min, and the second part over 22 min.

The long-term integrated values of Z_{DR} and L_{DR} are used to estimate the value of σ_δ. To this end, Z_{DR} and L_{DR} are tabulated for $\mu = 0$ and different values of D_0 and σ_δ, with D_0 changing in steps of 0.08 mm, and σ_δ in steps of 5°. Table 2 gives the integrated radar observables and derived σ_δ. Note that the spread of the canting-angle distribution is 30° for both parts, which is solely due to the 5° interval of the table entries. The actual values of σ_δ will differ somewhat: it is smaller in the first part of the measurement than it is in the second part. Beard and Jameson (1983) theoretically predict that the isotropic turbulence may only cause a σ_δ smaller than 10°, and not as large as 30°. However, during the radar measurements described in this paper, turbulence is not isotropic. Furthermore, the radar measurements were done above an urbanized area during strong wind. Saunders (1971) measured canting angles of raindrops near the surface and found that the spread of the distribution is of the order of 30°. Maher et al. (1977) showed that strong wind gusts may cause such large canting angles. Inferring the canting angle from radar measurements is based on the principle that particle canting increases L_{DR} and decreases Z_{DR}. However, drop vibrations have the same effect and therefore cannot be excluded: σ_δ may represent drop vibrations as well. It is important to note that with such large (apparent) canting angles small Z_{DR} values do not necessarily indicate small raindrops.

The selected D_0 is used to calculate W_d, and finally the spread W_t of the turbulence spectrum is estimated by means of

$$W_t^2 = \bar{W}_{d,m}^2 - W_d^2, \tag{21}$$

in which $\bar{W}_{d,m}$ is the long-term integrated width of the Doppler spectrum. The results are also given in Table 2. In the first half of the measurement, W_t equals 0.9 m s^{-1}, and in the second half, 1.3 m s^{-1}. After removal of turbulence, W_d equals 0.6 m s^{-1}. This value is in agreement with earlier measurements by Russchenberg and Ligthart (1989). There, it was based on the statistical distribution of measured values of W_d, during other, nonturbulent, events, whereas during this analysis it results after correction of a turbulent event.

The estimate of W_t is based on *long-term* integrated data but is used to correct *short-term* averaged data. The error ΔW_t of W_t is estimated by taking the statistical spread of Z_{DR} and $W_{d,m}$ into account, according to the following scheme:

$$\bar{Z}_{DR} + \frac{1}{2}\sigma_{Z_{DR}}|_{\bar{W}_{d,m}} \rightarrow W_{tt1} \tag{22}$$

$$\bar{W}_{d,m} + \frac{1}{2}\sigma_{W_{d,m}}|_{\bar{Z}_{DR}} \rightarrow W_{tt2} \tag{23}$$

$$\Delta W_t = 2[(W_t - W_{tt1})^2 + (W_t - W_{tt2})^2]^{1/2}. \tag{24}$$

TABLE 2. Results of long-term integration.

	First part	Second part
$\bar{Z}_{DR}$ (dB)	0.5	0.6
$\bar{L}_{DR}$ (dB)	−28.4	−26.0
D_0 (mm)	0.9	1.1
σ_δ	30°	30°
$\bar{W}_{d,m}$ m s^{-1})	1.1	1.4
W_d (m s^{-1})	0.6	0.6
W_t (m s^{-1})	0.9	1.3
$W_t - W_{tt1}$ (m s^{-1})	0.008	0.0012
$W_t - W_{tt2}$ (m s^{-1})	0.025	0.077
ΔW_t (m s^{-1})	0.052	0.156

Term W_{tt1} is the width of the turbulence spectrum that would be calculated if the standard deviation $\sigma_{Z_{DR}}$ of Z_{DR} were taken into account, and W_{tt2} would be calculated if the standard deviation $\sigma_{W_{d,m}}$ of $W_{d,m}$ were taken into account. Finally, the total error ΔW_t is taken as an rms value to get the worst-case estimation. Table 2 shows the results. The effect of Z_{DR} variations is very small; ΔW_t is almost entirely caused by W_{tt2}.

Finally, Z_{DR} and W_d are used to derive the drop size distribution for the short-term integrated data. To this end, Z_{DR} and W_d are tabulated for the earlier-derived $\sigma_\delta = 30°$; D_0 changes in steps of 0.08 mm, and μ changes from −3 to 10 with a step of 1. Figure 5 shows the resulting drop size distribution as function of time. The dispersion factor μ is not constant: it fluctuates between −2 and 9 (excluding the extreme values of the tables); D_0 fluctuates around 1 mm, while N_0 varies between 35 and 50 dB (0 dB = 1 mm^{-3} mm$^{-1-\mu}$). In the N_0 plot, an additional line is drawn at $N_0 = 39$ dB, which is the value of $N_0(\mu = 0)$ of the Marshall–Palmer distribution. Note that most of the time N_0 is larger than that. In the time frame between 40 and 60 min, μ and D_0 become large, while N_0 decreases. To exclude the influence of μ during that time interval, the calculation was repeated but with μ fixed to 0. It revealed a similar behavior: D_0 increases, while N_0 decreases. This effect is due to the combination of a large Z_{DR} and moderate Z_h: the large value of D_0 that results from Z_{DR} would normally correspond to a large Z_h, but since that has not been observed, a small N_0 is necessary for fitting the data.

7. Statistics of N_0, D_0, and μ

The dispersion factor was found to vary during the event, and most of the time μ was larger than 0. To illustrate the statistical distribution of the parameters of the drop size distribution, histograms of N_0, D_0, and μ are given in Fig. 6. Again, data with $\mu = -3$ or $\mu = 10$ are ignored.

The distribution of μ is peaked around $\mu = 0.6$, but the spread around the peak is considerable. The median

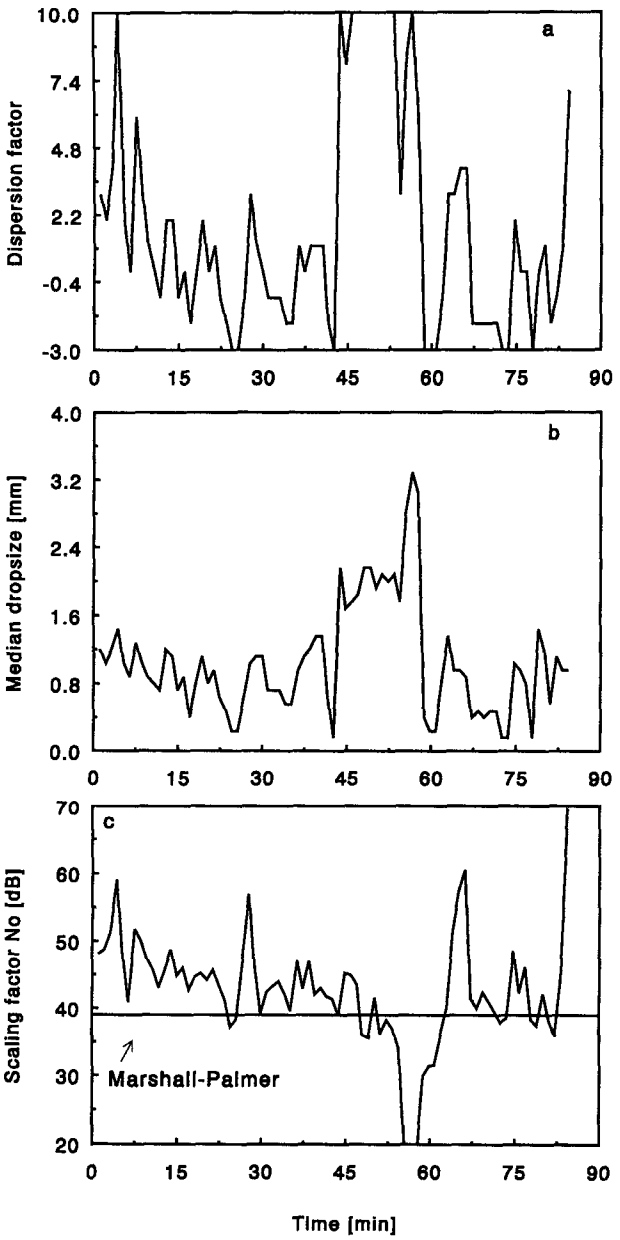

FIG. 5. Time dependence of the parameters of the drop size distribution after integration of the radar data over 1500 m and 64 s.

diameter D_0 is distributed between 0.5 mm and 1.5 mm. The scaling factor N_0 is distributed between approximately 39 and 54 dB, with a peak at 45 dB. Table 3 gives the mean and standard deviation of μ, D_0, and N_0. Also given are the mean and standard deviation of N_0 and D_0, in case $\mu = 0$.

Note that keeping μ constant reduces the scatter of N_0 by 4 dB. This is due to the dimensional relationship of N_0 and μ. It appears that the mean value of D_0 is larger when μ is kept to 0; the standard deviation is hardly affected. Table 4 shows the mean drop concentration N_t and total drop volume Vol_t, calculated with the mean values of N_0, D_0, and μ. Note that although the estimated number of drops differs substantially, the total drop volume does not differ much: approximately 3%.

The earlier-defined error ΔW_t of the width of the turbulence spectrum, due to variations of the radar

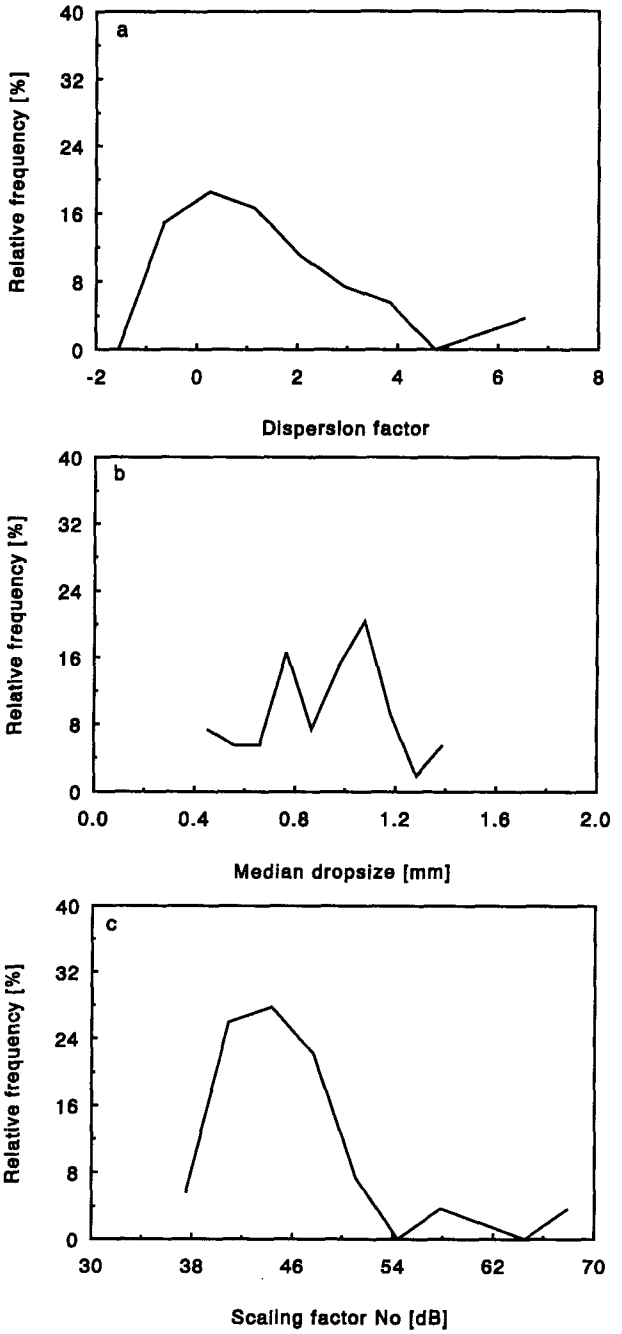

FIG. 6. Histograms of the dispersion factor μ, median drop size D_0, and scaling factor N_0.

observables, will also result in an error of the derived drop size distribution. To estimate the error, the procedure to calculate N_0, D_0, and μ was repeated with $W_t' = W_t + \frac{1}{2}\Delta W_t$, and $W_t' = W_t - \frac{1}{2}\Delta W_t$. The results are given in Table 5, where for ease of comparison the original values are given as well. The errors of μ and N_0 are not symmetric around the mean: overestimation of W_t results in a larger error than underestimation. The worst-case error neglects this asymmetry, because it is defined as twice the largest error.

8. On the relationship between N_0, D_0, and μ

The accuracy of single-parameter radars could be enhanced if possible interrelationships between the different parameters of the drop size distribution were taken into account. For instance, if N_0 and μ were related, a measurement of μ would imply N_0. When these two are incorporated into the Z–R relationship, the estimate of the rain intensity is improved. Ulbrich (1983) suggested such a relationship:

$$N_0 = C_N \exp(\beta\mu) \times 10^{-(1+\mu)} \quad (\mathrm{m}^{-3}\ \mathrm{mm}^{-1-\mu}). \quad (25)$$

Initially (25) was derived from data that spanned different rainfall types, and in that case β and C_N were found to be 3.2 and 6×10^{-4}, respectively. However, β and C_N may differ per event.

Figure 7 shows the scatter diagram of N_0 and μ, the regression line of the data, and (25) with the given values of β and C_N. The correlation coefficient of N_0 and μ is 0.84, which implies a significant relationship between the two. The observed relationship between N_0 and μ can be described with $\beta = 2.9$ and $C_N = 3 \times 10^5$. The regression line is given by

$$N_0 = 44.8 + 2.51\mu \pm 1.7 \quad (\mathrm{dB}). \quad (26)$$

It appears that the data are in reasonable agreement with (25). Note that (26) gives $N_0 = 44.8$ dB when $\mu = 0$, which is 5.8 dB larger than the value of N_0 that corresponds to the Marshall–Palmer distribution, whereas (25) results in 37.8 dB, which is 1.2 dB smaller.

The scatter diagram of D_0 and μ is given in Fig. 8. For $\mu < 3$, μ increases when D_0 increases. The width of the drop size distribution increases less with D_0 than it would in the case of a fixed μ. For $\mu \geq 3$, the data points are spread around $D_0 = 1$ mm. The observations are in agreement with those of Wessels (1972), who performed long-term measurements of drop size distributions using filter paper. In that experiment it was shown that although a different drop size distribution was used a shape factor similar to μ increased for rain intensities smaller than approximately 4 mm h^{-1} and decreased again for larger rain intensities. Also given in the figure is a third-order polynomial that relates μ to D_0:

$$D_0 = 0.97 + 0.14\mu - 0.043\mu^2 + 0.0033\mu^3 \pm 0.1 \text{ mm}. \quad (27)$$

TABLE 3. Mean and standard deviation of the parameters of the drop size distribution, derived with varying μ and with $\mu = 0$.

	μ	D_0 (mm)	N_0 (dB)	μ	D_0 (mm)	N_0 (dB)
Mean	0.6	0.9	45.6	0	1.2	36.4
Standard deviation	2.3	0.3	9.0	0	0.2	5.2

The measured N_0 and D_0 data were investigated for the presence of any correlation as well, but none was found. However, when the calculation of the drop size distribution was repeated with the assumption of $\mu = 0$, they were found to be negatively correlated with a coefficient of -0.68: N_0 tends to decrease with increasing rain intensity. Clearly, a varying μ decorrelates N_0 and D_0, because of the dimensional relationship of N_0 and μ.

9. The relationship between Z and R

The measured relationships between μ, N_0, and D_0 [Eqs. (26) and (27)] are incorporated into the expressions for Z and R; Z and R depend only on μ then. Second, the Z–R relationship is calculated by varying μ over the measured range of values. The resulting relationship can be expressed as a power law:

$$Z = 220R^{1.2} \quad (\mathrm{mm}^6\ \mathrm{m}^{-3}), \quad (28)$$

with R in millimeters per hour. Figure 9 shows the new Z–R relationship as well as the Marshall–Palmer relationship $Z = 200R^{1.6}$. Only $R < 10$ mm h^{-1} is shown, because the new Z–R relationship was derived from one particular, moderate, event. To arrive at (28) μ was varied from -2 to 6, with small values of μ causing the larger rain intensities. For $\mu < 0$ instabilities occurred, and extrapolation of the results of $\mu > 0$ was necessary.

The shapes of the curves are similar. For $R > 1$ mm h^{-1}, the new relationship predicts higher rain intensities than the Marshall–Palmer Z–R relationship. Chandrasekar and Bringi (1987) argued that using a *mean* relationship between N_0 and μ will not increase the accuracy of weather radars, because of the large sensitivity of Z and R to the, expected, variability of the N_0–μ relationship. The method described in this paper, however, enables the derivation of the N_0–μ relationship *per event;* the relationships between the pa-

TABLE 4. Drop concentration N_t (m^{-3}) and total drop volume V_t ($\mathrm{mm}^{-3}\ \mathrm{m}^{-3}$), calculated with constant or varying dispersion factor μ.

	N_t	V_t
$\mu = 0$	1.5×10^3	156.5
Varying μ	2.4×10^3	160.3

TABLE 5. Estimated error of the mean parameters of the drop size distribution due to the long-term integration of radar observables for turbulence correction.

Mean parameters	μ	D_0 (mm)	N_0 (dB)
$W_t' = W_t + \frac{1}{2}\Delta W_t$	1.9	1.0	46.1
$W_t' = W_t$	0.6	0.9	45.6
$W_t' = W_t - \frac{1}{2}\Delta W_t$	−0.3	0.8	43.7
Worst-case error	±1.3	±0.1	±1.9

rameters of the drop size distribution may differ per event, leading to different Z–R relationships.

10. Comparison with raingage measurements

To test the method of measuring the drop size distribution, the radar-derived rain intensity is compared with raingage data. The first range cell of the radar beam used for analysis is located at an altitude of 475 m, and the last one at 1225 m. The average altitude is 850 m. Horizontally, the raingage is located at a distance of approximately 1300 m from the center of the radar range used for the analysis.

Initially, the raingage data are integrated over 10 sec. To match the integration time of raingage data with that of the radar data, six samples are integrated; the 64-s-averaged value of the raingage data is estimated by means of linear interpolation of the 60-s data. Due to the different positions of the radar beam and raingage, the time lapse of the radar-derived rain intensity and the raingage result do not have to match; the raingage registration can be delayed with respect to the radar signal. The data have been corrected for this delay.

Figure 10 shows the time dependence of the rain intensity. The radar-derived rain intensity is calculated

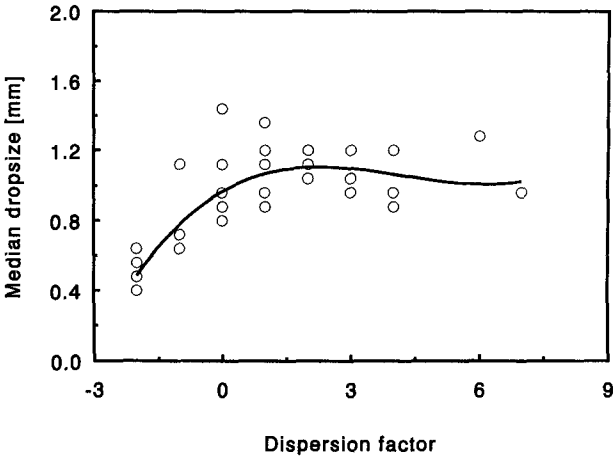

FIG. 8. Scatter diagram of the median drop size D_0 and dispersion factor μ.

in two ways: 1) only Z_{DR} is used with $\mu = 0$, and 2) W_d and Z_{DR} are used to incorporate variations of μ as well. The raingage did not register properly between 45 and 60 min. This is the same time interval as was excluded in the analysis of the previous sections, because of the risk of biasing the statistics due to the large Z_{DR}. Possibly, hydrometeors other than raindrops have been present in the radar beam during this interval.

The long-term averaged raingage data are converted to radar reflectivity with the Marshall–Palmer relationship and compared with the long-term averaged measured radar reflectivity; a small difference of 0.5 dB was found. In the first half of the measurement the temporal correlation between the raingage data and the radar data is good: all peaks coincide. In the second half of the measurement, after the rotation of the antennas, the raingage data are slightly delayed again; the radar beam was rotated away from the raingage. The

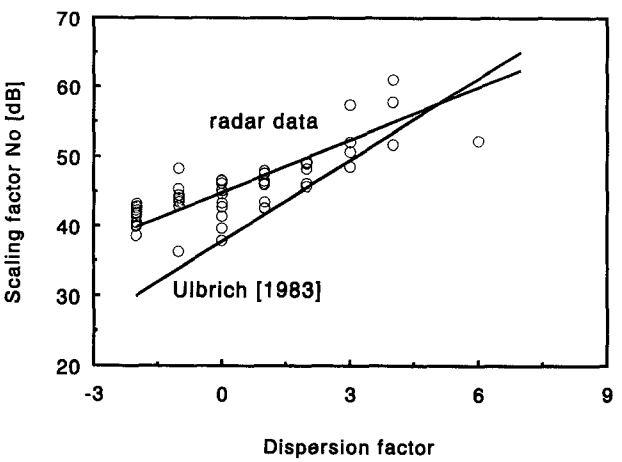

FIG. 7. Scatter diagram of the scaling factor N_0 and dispersion factor μ. Also given in the N_0–μ relationship of Ulbrich (1983), with $C_N = 6 \times 10^4$ and $\beta = 3.2$.

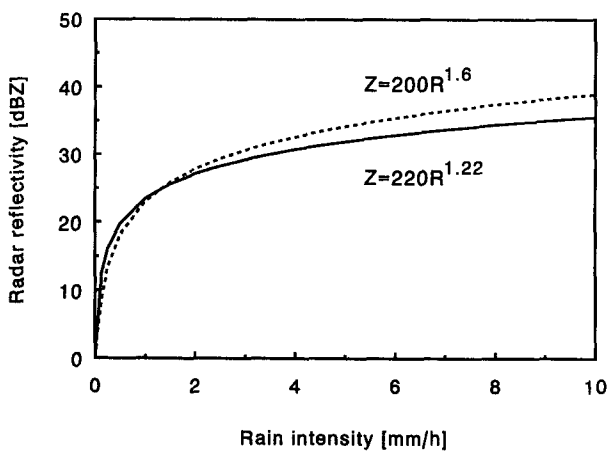

FIG. 9. Z–R relationships derived from the radar data and the Marshall–Palmer relationship.

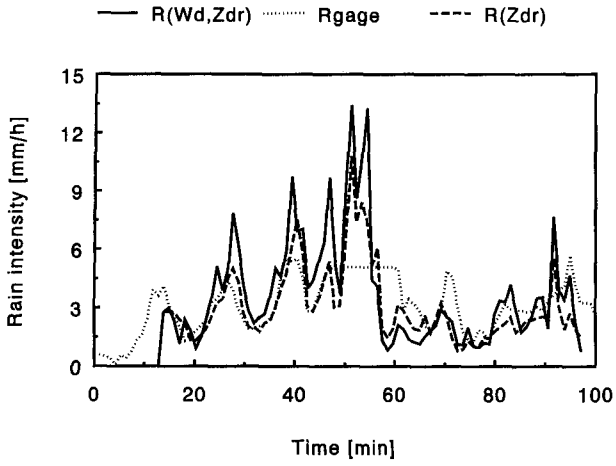

FIG. 10. The time dependence of the radar-derived rain intensities $R_{W_d,Z_{DR}}$, and $R_{Z_{DR}}$, and the raingage data. Integration time is 64 s. The raingage did not work properly between 45 and 60 min.

rain intensity that is derived with W_d and Z_{DR} is referred to as $R_{W_d,Z_{DR}}$. On average, it gives larger values than $R_{Z_{DR}}$ and R_{gage}.

Figure 11 shows the scatter diagrams of $R_{W_d,Z_{DR}}$, $R_{Z_{DR}}$, and R_{fit}, which result from (28), versus R_{gage}. Also given are the regression lines and the cross-correlation coefficients r. It appears that R_{fit} and $R_{Z_{DR}}$ are in good agreement with the raingage data but that $R_{W_d,Z_{DR}}$ is slightly larger than R_{gage}. The relative error Δ_R is estimated by

$$\Delta_R = \frac{\sum_i^N |R_{radar,i} - R_{gage}|}{\sum_i^N R_{gage}}. \quad (29)$$

The cross-correlation coefficients of the three scatter diagrams are of the same order of magnitude: 70%–75%. The relative errors are 52% for $R_{W_d,Z_{DR}}$, 23% for $R_{Z_{DR}}$, and 21% for R_{fit}. The accuracy of $R_{Z_{DR}}$ and R_{fit} is comparable; the inclusion of a variable μ does not seem to improve the radar estimation of the rain intensity. However, for larger rain intensities the scatter around the regression line is smaller in case of R_{fit} than in case of $R_{Z_{DR}}$. It is important to note that satisfactory results are obtained using large canting angles.

11. Conclusions

The combination of Z_h, Z_{DR}, and W_d can be used to calculate the three parameters of the gamma drop size distribution: μ, N_0, and D_0. The measured Doppler spectrum needs to be corrected for turbulence. The combination of Z_{DR} and L_{DR} is used to estimate the spread of the canting-angle distribution. The derived spread of 30° is much larger than theoretically predicted. As hypothesis it is advanced that the large spread may be caused by strong wind effects in the urbanized environment of the radar. It is found that N_0 and D_0 are strongly related to μ, although D_0 and N_0 are not related to each other. The measured relationship between N_0 and μ qualitatively agreed with the result of Ulbrich (1983). Incorporating the measured relationship between the parameters of the drop size distribution results in a Z–R relationship that differs from the Marshall–Palmer relationship. Comparison with raingage measurements revealed that the accuracy of

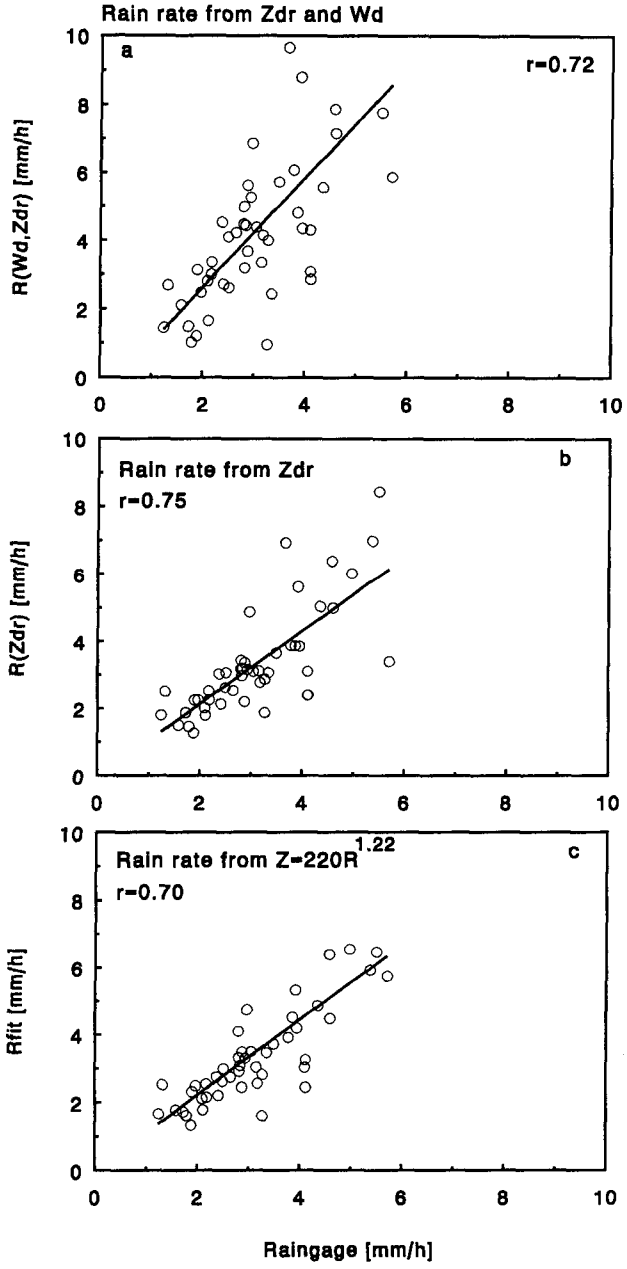

FIG. 11. Scatter diagrams of the radar-derived rain intensities versus the raingage measurements. Also shown are the regression lines and correlation coefficients r.

the radar-derived rain intensity was not significantly enhanced by the inclusion of μ. However, only a limited amount of data was analyzed, and the measurement configuration was not ideal: the raingage was not positioned underneath the radar beam. To study the accuracy of the method properly, a long-term measurement campaign is necessary.

Operational weather radars are not usually equipped with the capability to measure W_d and Z_{DR} and, therefore, will not be able to measure μ. In that respect the major conclusion of this paper is that interrelationships between the parameters of the drop size distribution exist that may improve the accuracy of the single-parameter radars. The limited amount of data that was analyzed in this paper spanned only rain intensities lower than 10 mm h^{-1} and was obtained during one event. More data are necessary to extend the operational use of this paper for different rain situations.

Acknowledgments. I would like to thank Professor Leo Ligthart for the fruitful discussions we had.

REFERENCES

Atlas, D., R. C. Srivastava, and R. S. Sekhon, 1973: Doppler radar characteristics of precipitation at vertical incidence. *Rev. Geophys. Space Phys.*, **11,** 1–35.

Battan, L. J., 1973: *Radar Observation of the Atmosphere.* The University Press of Chicago, 324 pp.

Beard, K. V., and A. R. Jameson, 1983: Raindrop canting. *J. Atmos. Sci.*, **40,** 448–454.

Bringi, V. N., T. A. Seliga, and S. M. Cherry, 1983: Statistical properties of the dual polarization reflectivity (Z_{DR}) radar signal. *IEEE Trans. Geosci. Remote Sens.*, **GE-21,** 215–220.

Brussaard, G., 1976: A meteorological model for rain-induced cross polarization. *IEEE Trans. Antennas Propag.*, **AP-24,** 5–11.

Chandrasekar, V., and V. N. Bringi, 1987: Simulation of radar reflectivity and surface measurements of rainfall. *J. Atmos. Oceanic Technol.*, **4,** 464–478.

Chu, Y. H., T. S. Hsu, L. H. Chen, and J. K. Chao, 1990: The investigations of the atmospheric precipitations by using Chung-Li VHF radar. *Radio Sci.*, **26,** 717–729.

Doviak, R. J., and D. S. Zrnić, 1984: *Doppler Radar and Weather Observations.* Academic Press Inc., 458 pp.

Frost, I. R., J. W. F. Goddard, and A. J. Illingworth, 1991: Hydrometeor identification using cross-polar radar measurements and aircraft verification. *Proc. 25th Conf. on Radar Meteorology,* Paris, Amer. Meteor. Soc.

Fujita, M., K. Nakamura, H. Inomata, and K. Okamoto, 1989: Intercomparison of radar measurements of rain by single- and dual-wavelength techniques. *Radio Sci.*, **24,** 65–75.

Goddard, J. W. F., and S. M. Cherry, 1984: Quantitative precipitation measurements with dual linear polarisation radar. *Proc. 22nd Conf. of Radar Meteorology,* Amer. Meteor. Soc.

Hauser, D., and P. Amayenc, 1981: A new method for deducing hydrometeor-size distributions and vertical air motions from Doppler radar measurements at vertical incidence. *J. Appl. Meteor.*, **20,** 548–555.

Joss, J., and E. G. Gori, 1978: Shapes of raindrop-size distributions. *J. Appl. Meteor.*, **17,** 1054–1061.

Klaassen, W., 1989: Determination of rain intensity from Doppler spectra of vertically scanning radar. *J. Atmos. Sci.*, **6,** 552–562.

Maher, B. O., P. J. Murphy, and M. C. Sexton, 1977: A theoretical model of the effect of wind gusting on rain-induced cross-polarization. *Ann. Telecom.*, **32,** 404–408.

Pruppacher, H. R., and R. L. Pitter, 1971: A semi-empirical determination of the shape of cloud and rain drops. *J. Atmos. Sci.*, **28,** 86–94.

Russchenberg, H. W. J., 1992: *Ground-based Remote Sensing of Precipitation with a Multi-polarised FM-CW Doppler Radar.* Delft University Press, 206 pp.

——, and L. P. Ligthart, 1989: Doppler-polarimetric research of precipitation with the Delft Atmospheric Research Radar, Final Report for the European Space Agency under contract no. 6814/86/NL/PB(SC), ESTEC, Noordwijk, the Netherlands.

Saunders, M. J., 1971: Cross polarization at 18 and 30 GHz due to rain. *IEEE Trans. Antennas Propag.*, **19,** 273–277.

Seliga, T. A., and V. N. Bringi, 1976: Potential use of radar differential reflectivity measurements at orthogonal polarizations for measuring precipitation. *J. Appl. Meteor.*, **15,** 69–75.

Steiner, M., 1991: A new relationship between mean Doppler velocity and differential reflectivity. *J. Atmos. Oceanic Technol.*, **8,** 430–441.

Steinhorn, I., D. S. Zrnić, 1988: Potential uses of the differential propagation phase constant to estimate raindrop and hailstone size distributions, *IEEE Trans. Geosci. Remote Sens.*, **26.**

Ulbrich, C. W., 1983: Natural variations in the analytical form of the raindrop size distribution. *J. Climate Appl. Meteor.*, **22,** 1764–1775.

Wessels, H. R. A., 1972: Measurements of raindrops (Metingen van regendruppels, in Dutch), Scientific report WR 72-6, Royal Dutch Meteorological Institute, De Bilt, the Netherlands.

Woodman, R. F., and Y. H. Chu, 1989: Aspect sensitivity measurements of VHF backscatter made with the Chung-Li radar: Plausible mechanisms. *Radio Sci.*, **24,** 113–125.